

CFAR TARGET DETECTION IN GROUND SAR IMAGE BASED ON KK DISTRIBUTION

Yanzhao Gao^{*}, Ronghui Zhan, Jianwei Wan, Jiemin Hu, and Jun Zhang

ATR Key Laboratory, School of Electronic Science and Engineering, National University of Defense Technology, Changsha 410073, China

Abstract—This paper deals with the problem of constant false alarm rate (CFAR) target detection in high-resolution ground synthetic aperture radar (SAR) images based on KK distribution. For the parameter estimation of KK distribution, the semi-experiential algorithm is analyzed firstly. Then a new estimation algorithm based on the particle swarm optimization (PSO) is proposed, which takes the discrepancies between the histogram of the clutter data and probability density function (PDF) of KK distribution at some selected points as the cost function to search for the optimal parameter values using PSO algorithm. The performance of the two algorithms is compared using Monte-Carlo simulation using the simulated data sets generated under different conditions; and the estimation results validate the better performance of the new algorithm. Then the KK distribution, which is proposed for spiky sea clutter originally, is applied to model the real ground SAR clutter data. The goodness-of-fit test clearly show that the KK distribution is able to model the ground SAR clutter much better than some common used model, such as standard K-distribution and Gamma, etc. On this basis, a global CFAR target detection algorithm is presented. The detection threshold is calculated numerically through the cumulative density function (CDF) of KK distribution. Comparing the amplitude of every SAR image pixel with this threshold, the potential targets in ground SAR images can be located effectively. Then target clustering is implemented to eliminate the false alarm and obtain more accurate target regions. The detection results of the proposed algorithm in a typical ground SAR image show that it has better performance than the detector based on G^0 distribution.

Received 16 March 2013, Accepted 7 May 2013, Scheduled 19 May 2013

* Corresponding author: Yanzhao Gao (buaagaoyz@sina.com).

1. INTRODUCTION

With the rapid development in the past years [1–5], the high-resolution SAR is capable of producing very high quality images. It is reported that typical sensor platforms is able to provide wide area search coverage (approximately 100 km^2 area per minute) at $1.0 \text{ m} \times 1.0 \text{ m}$ resolution [6]. This attractive capability has opened new interesting research fields in both civil and military contexts, such as target detection [7, 8], target recognition [9, 10], navigation [11], etc.. Target detection is one of the core applications of SAR remote sensing and has received considerable attentions in the recent years, such as CFAR method [12–18], the GLRT method [19], the extended fractal-based method [20], the wavelet transform-based method [21], etc.. Among these kinds of methods, the CFAR method has been most widely used for it is capable of maintaining the constant false alarm probability at a certain level in non-stationary background through an adaptive threshold. The commonly used CFAR detection algorithms include the cell-average CFAR (CA-CFAR), greatest-of CFAR (GO-CFAR), smallest-of CFAR (SO-CFAR), order statistic CFAR (OS-CFAR), etc.. In general, a practical CFAR detector is a compromise of three aspects, i.e., executive speed, detection precision and feasibility. Up to now, the global CFAR detector based on the statistical character of the background, which is actually a kind of CA-CFAR detector, is one of the most practical CFAR algorithms in despite of its disadvantages [22]. It is considered in this algorithm that the target pixels account for a very small proportion in the SAR images. As a result, the presence of the target has scarcely any influence on the statistical characteristic of the background. If the clutter background of the whole images could be modeled accurately, it is easy to find out the brighter pixels, which corresponding to the targets. This algorithm is simple to implement and has low computational burden.

The CFAR detectors are based on a Neyman-Pearson likelihood criterion, which requires the specification of an appropriate statistical clutter model for the detection performance. An excellent statistical clutter model should provide a good fitting to SAR image clutter in many practical scenarios. Unfortunately, less attention has been devoted to land scattering in high-resolution SAR, while many investigations have been carried out in the statistical analysis and modeling of high-resolution ocean SAR images [23–26]. Actually, as the same as the sea clutter, the statistics of the SAR image clutter of the ground areas depends on many complicated factors, such as the radar's operating mode, grazing angle and background operating environment, etc.. As a result, it is very hard to found a universal model for all

kinds of ground SAR clutter. A class of G distributions is presented for the extremely heterogeneous clutter in [27], and its special case, G^0 distribution, has been successfully applied to target detection scheme design [28]. It is validated that the GK and LNT distributions are the best models for some of the MSTAR ground SAR clutter among the compared models [23]. In this paper, the KK distribution [29], which is originally presented to model the heavy spikes in sea clutter as an alternative to the KA distribution, is applied to model the ground SAR image clutter.

As far as a parametric clutter model is concerned in target detection schemes, the parameter estimation is an indispensable step; since the PDF estimation problem is formulated as a parameter estimation one. For the parameter estimation of KK distribution, a semi-exponential algorithm is presented based on some real X-band, high-resolution and high grazing clutter sea clutter data sets, and its good performance for these clutter data sets has been already validated [29]. This algorithm, however, is based on two basic hypotheses: 1) the mixing coefficient is selected exponentially according to the characteristic of the data set and the spiky component of the KK distribution is very small; 2) the shape parameters of the two K components are considered to be equal. Actually, these two hypotheses may be not reasonable for clutter obtained under different conditions. A small mixing coefficient would weaken the capability of KK distribution to model the spike in clutter. In this paper, a new algorithm based on the PSO is proposed, which takes the discrepancies between the histogram of the clutter data and probability density function of KK distribution at some selected points as the cost function to search for the optimal parameter values using PSO algorithm. This algorithm is capable of estimating the parameter of KK distribution without any pre-knowledge of the clutter.

The main contributions of the paper are threefold: 1) a new parameter estimation algorithm for KK distribution is presented; 2) the KK distribution is applied to model the ground SAR image; 3) a global CA-CFAR target detection algorithm based on KK distribution is proposed in ground SAR images.

The remainder of this paper is organized as follows. The KK distribution is introduced in Section 2. The parameter estimation of KK distribution, including the semi-exponential algorithm and the new algorithm, is studied in Section 3. Then a CFAR detector based on KK distribution is proposed in Section 4, followed by concluding remarks in Section 5.

2. THE KK DISTRIBUTION

At a low grazing angle, the K distribution has been validated in many literatures that it is a proper model for the high-resolution sea clutter returns [30, 31], which are subjected to shadowing, ducting and multipath propagation [29, 32]. By contrast, the returns are affected by Bragg scattering from rough sea surface and scattering from whitecaps at higher grazing angles [29]. In this case the K distribution is no longer a sufficient model because of the severe spike in clutter. The KA distribution is presented to improve the adaptability to the sea clutter distribution particularly in the tail region in [33, 34]. However, the KA distribution cannot be expressed in closed form, and its PDF and CDF have to be numerically computed, which absolutely increases the difficulty for the analysis of the radar detection performance. As an alternative, the KK distribution is proposed to model the sea clutter distribution of high grazing angles in [29], where both the Bragg/whitecap scatters and spikes are assumed to be K distribution. The overall clutter distribution is the mixture of the two K distribution, i.e.,

$$f_{KK}(x) = (1 - k) f_{K_1}(x; v_1, b_1) + k f_{K_2}(x; v_2, b_2) \quad (1)$$

where f_{K_1} and f_{K_2} are both K distribution with parameters as specified characterized by the densities

$$f_{K_j}(x; v_j, b_j) = \frac{2}{b_j \Gamma(v_j)} \left(\frac{x}{2b_j} \right)^{v_j} K_{v_j-1} \left(\frac{x}{b_j} \right), \quad (2)$$

$$x \geq 0, v_j \geq 0, b_j \geq 0, j = 1, 2$$

where v_j and b_j are the shape and scale parameters, respectively, and $K_{v_j-1}(\cdot)$ is a modified Bessel function. The first K distribution f_{K_1} in (1), which is called K_1 component in this paper, represents the Bragg/whitecap scatters, and the second K distribution f_{K_2} in (1), which is called K_2 component, represents the spike component. $k \in [0, 1]$ is the mixing coefficient. If $k = 0$, $f_{KK}(x) = f_K$ and it simplifies to the standard K distribution without the spike component.

The n th moment of KK distribution in (1) is given by

$$E\{X^n\} = (1 - k) \frac{2^n \Gamma(n/2 + 1) b_1^n \Gamma(v_1 + n/2)}{\Gamma(v_1)} + k \frac{2^n \Gamma(n/2 + 1) b_2^n \Gamma(v_2 + n/2)}{\Gamma(v_2)}. \quad (3)$$

The CDF of KK distribution can be obtained from the fact that

$$F_{KK}(x) = (1-k)F_{K_1}(x) + kF_{K_2}(x) = (1-k) \left[1 - \frac{2}{\Gamma(v_1)} \left(\frac{x}{2b_1} \right)^{v_1} K_{v_1} \left(\frac{x}{b_1} \right) \right] + k \left[1 - \frac{2}{\Gamma(v_2)} \left(\frac{x}{2b_2} \right)^{v_2} K_{v_2} \left(\frac{x}{b_2} \right) \right] \quad (4)$$

where $F_{K_1}(x)$ and $F_{K_2}(x)$ represent CDF of the component K_1 and K_2 , respectively.

Let $\mathbf{x}_{KK}^{(k)} = \{x_i | i = 1, 2, \dots, N\}$ denotes a group of clutter data obeys KK distribution with mixing coefficient k and sample size N . A simulated clutter data set $\mathbf{x}_{KK}^{(0.2)}$ is generated with the parameters with $N = 10000$, $v_1 = v_2 = 2$, $b_1 = 5$ and $b_2 = 20$. The histogram of the data set is plotted in Fig. 1 along with the corresponding KK distribution and K_1 component. From Fig. 1, it is seen that the PDF of KK distribution has a heavier tail than K distribution, which means that it is capable of modeling much more spiky clutter.

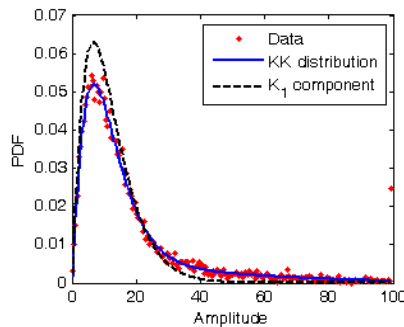


Figure 1. The histogram of data set \mathbf{x} and the corresponding KK distribution and K_1 component.

3. PARAMETER ESTIMATION OF KK DISTRIBUTION

3.1. Semi-experiential Algorithm

The semi-experiential algorithm[†] is proposed by Dong in [29] based on the analysis of an X-band, high-resolution and high grazing clutter data set. There are two basic hypotheses in this algorithm as have been already summarized previously: 1) the mixing coefficient is selected experientially; 2) the shape parameters of the two K components are

[†] This algorithm is named by the authors of this paper according to its characteristic.

considered to be equal, i.e., $v_1 = v_2$. On this basis, the estimation procedure of the five parameters of KK distribution is divided into three steps: 1) select the mixing coefficient k experientially according to the characteristic of the data set; 2) estimate the parameters \hat{v} , \hat{b} of the K distribution in (2) from the data set and assign them to the K_1 component of KK directly, i.e., $v_1 = v_2 = \hat{v}$, $b_1 = \hat{b}$; 3) estimate the scale parameter b_2 of K_2 component by making use of the discrepancies of the CDF of K and KK distribution.

In [29], the mixing coefficient is selected as $k = 0.01$ based on the statistical character of the given data set, and it is validated this algorithm is effective. However, for the radar clutter data obtained under different conditions, the coefficient k is very hard to select quickly and accurately. Up to now, there is no effective method to select k automatically. The discrepancies between the KK distribution and its K_1 component increase if the value of k is getting larger. As a result, it is not reasonable to assign the parameter value of K distribution to the K_1 component in step 2) when k is no longer as small as 0.01.

In order to illuminate the errors arisen from assigning the estimates \hat{v} and \hat{b} to the parameters of K_1 component in step 2) directly, 8 groups of clutter data $x_{KK}^{(k)}$ are generated with different k and $v_1 = v_2 = 2$, $b_1 = 5$, $b_2 = 20$, $N = 10000$. The parameters of K distribution are estimated through the method in [35] based on the data sets. Then the errors between the estimates (\hat{v} and \hat{b}) and the true parameter values of the K_1 component ($v_1 = 2$, $b_2 = 5$) are calculated using Monte-Carlo simulation. The results are given in 2 by means of the mean error (ME) and root mean square error (RMSE), which are defined as

$$\text{ME} = \frac{1}{M} \sum_{m=1}^M \hat{\theta}_m - \theta, \quad (5)$$

$$\text{RMSE} = \sqrt{\frac{1}{M} \sum_{m=1}^M (\hat{\theta}_m - \theta)^2} \quad (6)$$

where θ denotes the true parameter value of K_1 component, and $\hat{\theta}_m$ is the m th estimate result.

From Table 1, it can be seen that the MEs and RMSEs increase, especially the scale parameter b_1 , while k changes from 0.01 to 0.7. As a result, it is improper to assign \hat{v} and \hat{b} to the parameter of K_1 component directly when k is large, which means the performance of the semi-experiential algorithm is bad.

Table 2–Table 4 list the estimation errors of b_2 based on three

Table 1. The estimation errors of parameter v_1 and b_1 of KK distribution with different k .

k	ME		RMSE	
	v_1	b_1	v_1	b_1
0.01	-0.2099	0.4690	0.0830	0.1521
0.10	-1.0102	4.9520	0.0204	0.1897
0.20	-1.2130	9.3150	0.0136	0.2494
0.30	-1.3027	13.9721	0.0111	0.3595
0.40	-1.3416	18.6180	0.0082	0.4229
0.50	-1.3292	23.1933	0.0094	0.4212
0.60	-1.3292	27.2050	0.0097	0.4524
0.70	-1.2735	30.0711	0.0118	0.4705

Table 2. The estimation errors of b_2 based on data set $\mathbf{x}_{KK}^{(0.01)}$ for different k .

	$k = 0.01$	$k = 0.10$	$k = 0.20$	$k = 0.30$	$k = 0.40$	$k = 0.50$	$k = 0.60$
ME	0.9754	-4.9856	-6.0036	-6.5408	-6.9172	-7.3067	-7.3874
RMSE	1.0803	0.6945	0.7625	0.6739	0.7097	0.6291	0.7070

Table 3. The estimation errors of b_2 based on data set $\mathbf{x}_{KK}^{(0.3)}$ for different k .

	$k = 0.01$	$k = 0.10$	$k = 0.20$	$k = 0.30$	$k = 0.40$	$k = 0.50$	$k = 0.60$
ME	22.4356	9.0053	6.8776	5.5413	4.5917	4.0077	3.7935
RMSE	1.3339	0.9673	0.8174	0.7363	0.7245	0.7214	0.7743

Table 4. The estimation errors of b_2 based on data set $\mathbf{x}_{KK}^{(0.6)}$ for different k .

	$k = 0.01$	$k = 0.10$	$k = 0.20$	$k = 0.30$	$k = 0.40$	$k = 0.50$	$k = 0.60$
ME	9.1586	6.2581	5.5314	4.9443	4.6067	4.7659	4.6198
RMSE	13.2887	2.8818	2.0111	1.7421	1.8235	1.8378	2.0355

data sets $\mathbf{x}_{KK}^{(0.01)}$, $\mathbf{x}_{KK}^{(0.3)}$, $\mathbf{x}_{KK}^{(0.6)}$, respectively. In each table, the k is pre-selected arbitrarily as $k = 0.01, 0.10, 0.20, \dots, 0.60$ in the estimation of b_2 . From the three tables along with Table 1, it can be seen that the performance of semi-experiential algorithm is bad especially when k is selected improperly. In Table 2, the results for $k = 0.01$ is acceptable, which is exactly the instance in [29].

3.2. Parameter Estimation Algorithm Based on PSO

The PSO algorithm, which is an evolution algorithm based on swarm intelligence, was presented by J. Kennedy and R. Eberhart in 1995 [36]. It is capable of solving the global optimal solution of non-linear and non-differentiable problem and has been received considerable attentions [37–39]. The PSO is initialized with a population of random particles, and each particle is treated as a solution with two states: the current position $\mathbf{x}_i = (x_{i1}, x_{i2}, \dots, x_{iD})$ and the current velocity $\mathbf{v}_i = (v_{i1}, v_{i2}, \dots, v_{iD})$ in a D -dimensional space. The fitness of each particle is evaluated by the cost function and its current position. Simultaneously, the orientation and displacement of each particle is decided by its velocity. Each particle keeps track of its coordinates in hyperspace which are associated with the best solution, which makes the cost function minimum, it has achieved so far. This value is called *pbest* denoted as $pbest = (p_{i1}, p_{i2}, \dots, p_{iD})$. The “global” version of the particle swarm optimizer keeps track of the overall best value obtained thus far by any particle in the population, which is called *gbest* denoted as $gbest = (g_1, g_2, \dots, g_D)$.

At each iterative step, the particles change their positions and velocities toward the *pbest* and *gbest*. In the $(k + 1)$ step, for example, the position and velocity of each particle is updated using following formulas,

$$v_i^{k+1} = wv_i^k + c_1r_1(p_{i,j} - x_{i,j}^k) + c_2r_2(g_i - x_{i,j}^k), \quad (7)$$

$$x_{i,j}^{k+1} = x_{i,j}^k + v_{i,j}^k \quad (8)$$

where w is the inertial weight, c_1 and c_2 are the acceleration constants, r_1 and r_2 are random numbers uniformly generated from $[0, 1]$.

In the PSO algorithm, the fitness of each particle is evaluated by its cost function. An efficient cost function has intense influence on the convergence speed and precision of the algorithm. The maximum likelihood function [40], the equivalence of theoretical and experimental statistical moments [41] and the second-kind cumulants [42] are commonly used for the parameter estimation of the clutter models. For the KK distribution, however, these are not appropriate because 1) the maximum likelihood function and the second-kind cumulants is very complicated; 2) the KK distribution has heavy tail in its PDF, which results in severe departure between the theoretical moments and statistical moments especially when the moment order is high as the same as the Pareto distribution [43]. The discrepancy between the histogram of the clutter data and PDF of KK distribution are considered as the cost function in this paper. Least-square fitting is applied at specifically selected points of the histogram of the clutter

data and the PDF of KK distribution. A total of G points are sampled in this paper; and the cost function is given as,

$$f_{cost} = \sum_{g=1}^G (f_{KK}(g) - h(g))^2 \quad (9)$$

where $f_{KK}(g)$ and $h(g)$ denote the amplitude of the g th special point of the KK PDF and the amplitude of the same sample of the histogram of the clutter data, respectively. Minimizing the cost function, which means that the histogram of the clutter data is the most close to the PDF of KK distribution in amplitude domain, the parameters of KK distribution can be estimated, i.e.,

$$\boldsymbol{\theta} = \arg \min_{\boldsymbol{\theta}} \sum_{g=1}^G (f_{KK}(g) - h(g))^2 \quad (10)$$

where $\boldsymbol{\theta} = [k, v_1, b_1, v_2, b_2]^T$ denotes the parameter vector of the KK distribution. The estimation algorithm is summarized as the following steps.

- Step 1)** Initialize the parameters of the PSO algorithm, such as the size of random particles, the inertial weight w , the acceleration constants c_1 and c_2 , the maximum iterative time L , etc.. At the beginning, set the initial iterative time as $l = 1$.
- Step 2)** Generate the initial population of random particles $\Theta = \{\boldsymbol{\theta}_i | i = 1, 2, \dots, I\}$, where $\boldsymbol{\theta}_i = [k^{(i)}, v_1^{(i)}, b_1^{(i)}, v_2^{(i)}, b_2^{(i)}]^T$ denotes the position vector of the i th particle.
- Step 3)** Calculate the fitness of each particle according to (9).
- Step 4)** Compare the fitness of each particle with its own best solution $pbest$ and the global best solution $gbest$ obtained so far and update the two kinds of best solutions.
- Step 5)** Update the positions and velocities of the particles according to (7) and (8).
- Step 6)** Back to Step 3) while the iterative number $l < L$ and finish the optimization process if $l = L$.

It is reasonable to image that the smoothness of the histogram has intense influence on the precision of the estimation for the discrepancies between the histogram of the clutter data and probability density function of KK distribution is taken as the cost function. The smoothness of the histogram is mainly decided by two factors, i.e., the size of the clutter data N and the statistical interval δ . The larger the data size is, the smoother the histogram is, and so is the statistical

interval. In order to validate the influence of these two factors, two experiments are carried out based on the data set $\mathbf{x}_{KK}^{(0.2)}$. Table 5 lists the estimation errors for different sample sizes with invariable statistical interval $\delta = 2.0$; and the estimation errors for different statistical interval with a sample size $N = 10000$ are listed in Table 6. These results are also given by means of ME and RMSE in (5) and (6). It can be seen apparently that when the sample size and the statistical interval increase, which means the histogram of the clutter data is smoother, the entire MEs and RMSEs decrease, i.e., the estimation precision becomes higher.

Table 5. The estimation errors of the proposed algorithm for different sample size.

sample size	ME					RMSE				
	k	v_1	v_2	b_1	b_2	k	v_1	v_2	b_1	b_2
1000	0.0242	0.3001	0.1642	-0.2267	-1.0857	0.0765	0.6408	0.6554	0.9433	2.1028
2000	0.0235	0.2216	0.1445	-0.1803	-0.6107	0.0686	0.5186	0.7004	0.7839	1.5617
5000	0.0140	0.0989	0.0995	-0.0707	-0.3350	0.0536	0.3536	0.6004	0.5657	1.6367
10000	0.0078	0.0464	0.0985	-0.0078	-0.2819	0.0440	0.2674	0.5263	0.4202	1.4116

Table 6. The estimation errors of the proposed algorithm for different statistical interval.

statistical interval	ME					RMSE				
	k	v_1	v_2	b_1	b_2	k	v_1	v_2	b_1	b_2
0.2	0.0313	0.3623	0.1919	-0.3774	-1.3491	0.0713	0.6029	0.6130	0.9115	2.6377
0.5	0.0086	0.1418	0.1551	-0.1068	-0.7881	0.0473	0.4482	0.5715	0.6818	2.0494
1.0	0.0081	0.0949	0.1503	-0.0849	-0.7013	0.0450	0.3063	0.5665	0.5540	1.8786
2.0	0.0078	0.0464	0.0985	-0.0078	-0.2819	0.0440	0.2674	0.5263	0.4202	1.4116

The semi-experiential algorithm is affected strongly by the value of k as shown in Table 1–Table 4. In order to investigate the performance of the proposed algorithm for different k , the five parameters are estimated based on the data sets $\mathbf{x}_{KK}^{(0.01)}$, $\mathbf{x}_{KK}^{(0.2)}$, $\mathbf{x}_{KK}^{(0.4)}$, $\mathbf{x}_{KK}^{(0.6)}$, and the MEs and RMSEs are given in Table 7. From Table 7, it can be seen that the MEs and RMSEs do not change evidently when k increases from 0.01 to 0.60, which means the proposed estimation algorithm is robust for different clutter data sets.

Although the KK distribution is proposed for the spiky sea clutter

Table 7. The estimation errors of the proposed algorithm for different k .

k	ME					RMSE				
	k	v_1	v_2	b_1	b_2	k	v_1	v_2	b_1	b_2
0.01	0.0165	0.1583	-1.5599	-0.1286	-8.3819	0.0099	0.2687	0.1349	0.3611	5.5782
0.2	0.0067	0.0455	-0.0568	-0.0490	-0.2791	0.0315	0.2060	0.4526	0.3967	1.2724
0.4	0.0043	0.0419	-0.2173	-0.0224	-0.6034	0.0307	0.2554	0.4854	0.4644	1.6312
0.6	0.0014	0.1243	0.0907	-0.0532	-0.1843	0.0363	0.4202	0.4308	0.8117	1.6091

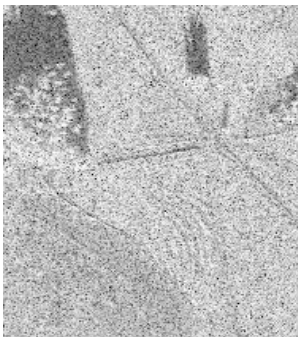


Figure 2. Grass field of the HB06171 file.

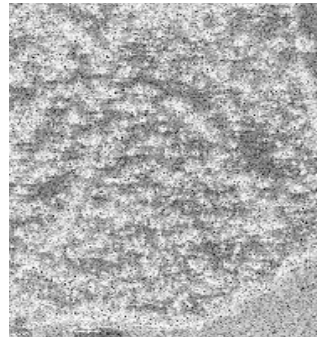


Figure 3. Wood field of the HB06192 file.

originally, it is capable of modeling clutter of some ground SAR images because of the heavy tail in its PDF. Two clutter files of the MSTAR SAR images [23], named HB06171 and HB06192 as show in Fig. 2 are Fig. 3, are tried to be modeled by KK distribution. The results of statistical analysis performed by commonly used clutter models, such as K distribution, Gamma distribution, G^0 distribution etc., are compared with KK distribution in Fig. 4 and Fig. 5.

The PDF expressions of G^0 distribution and Gamma distribution along with their moments of different order are given as follows, respectively.

G^0 model:

$$f_{G_0}(x) = \frac{2n^n \Gamma(n - \alpha) \gamma^{-\alpha} x^{2n-1}}{\Gamma(n) \Gamma(-\alpha) (\gamma + nx^2)^{n-\alpha}}, \quad -\alpha, \gamma, n, x > 0, \quad (11)$$

$$E \{X^r\} = (\gamma/n)^{r/2} \frac{\Gamma(-\alpha - r/2) \Gamma(n + r/2)}{\Gamma(-\alpha) \Gamma(n)}. \quad (12)$$

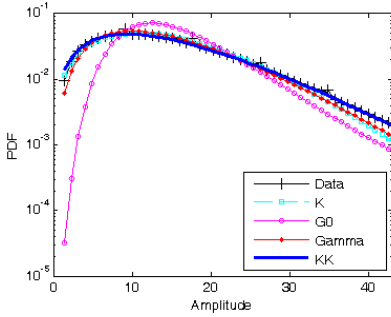


Figure 4. Amplitude histogram for image HB06171.

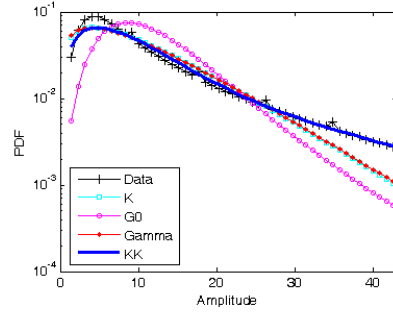


Figure 5. Amplitude histogram for image HB06192.

Table 8. Parameter estimation results of the clutter models.

File name	KK					K		G ⁰			Gamma	
	\hat{k}	$\hat{\nu}_1$	$\hat{\nu}_2$	\hat{b}_1	\hat{b}_2	$\hat{\nu}$	\hat{b}	$\hat{\alpha}$	$\hat{\gamma}$	\hat{n}	\hat{a}	\hat{b}
HB06171	0.1657	2.6115	2.5365	5.5407	5.9435	13.681	2.2834	-3.4633	738.845	2.9975	2.9975	5.0031
HB06192	0.2474	1.5443	2.2365	4.3648	1.0062	1.7555	4.8663	-2.8083	365.752	1.5514	1.5515	7.1484

Table 9. Goodness-of-fit test for grass field.

	K	G ⁰	Gamma	KK
K-S test	0.02018	0.05254	0.0225	0.01251
χ^2 test	0.2500	4.5770	1.5040	0.0150

Gamma model:

$$f_{Gamma}(x) = \frac{1}{b^a \Gamma(a)} x^{a-1} \exp(-\frac{x}{b}), \quad x > 0, \quad (13)$$

$$E\{X^r\} = \frac{b^r \Gamma(a+r)}{\Gamma(a)}. \quad (14)$$

Table 8 lists the parameter estimation results of the clutter models. From Fig. 4 and Fig. 5, it is seen that the KK distribution can fit SAR background clutter of grass field (HB06171) and wood field (HB06192) much better than other models, especially in the tail region. Goodness-of-fit tests are used to demonstrate the performance of the KK model along with the K distribution, G⁰ distribution and Gamma distribution and their fit to the experimental histograms. The chi-squared test and K-S test [41] are employed for this purpose. Table 9 and Table 10 list

Table 10. Goodness-of-fit test for wood field.

	K	G ⁰	Gamma	KK
K-S test	0.03042	0.05127	0.02879	0.009962
χ ² test	4.0030	8.7160	3.7210	0.000213

the goodness-of-fit test results. It is obvious from these results that the KK distribution is the best model, and the proposed parameter estimation algorithm has excellent performance for the SAR clutter data.

4. CFAR TARGET DETECTION ALGORITHM

The CFAR detectors make use of the distinction between the background noise or clutter power and the potential targets in brightness; and thus to maintain an approximately constant false alarm rate by adaptively changing the detection threshold. Theoretically, the optimal decision whether a pixel of the SAR image belongs to target or not can be made by Bayes rule. However, for 1) it is very hard to obtain prior probability of the targets; 2) the probability that the pixel belongs to target is far smaller than the one it belongs to background, it is more reasonable to adopt the Neyman-Pearson rule to make the decision,

$$\Lambda(x) \triangleq \frac{f_t(x)}{f_b(x)} > \frac{f_b(T)}{f_t(T)} \tag{15}$$

where x is the amplitude of a single pixel, and $f_t(\cdot)$ and $f_b(\cdot)$ denote the target and background PDF, respectively. T is the detection threshold, which is decided by the false alarm rate P_f :

$$P_f = \int_T^\infty f_b(x)dx. \tag{16}$$

Actually, the target pixels account for only a very small proportion in the SAR images, which makes it hard to obtain the statistical characters of the target pixels. As a result, a sub-optimal detection strategy is often adopted, i.e., if

$$f_b(x) > f_b(T) \tag{17}$$

the current pixel is judged as a target one.

In this paper, the KK distribution is used to model the background and the global CFAR detector based on the statistical character of the background is employed to detect potential targets in ground SAR

images. The relationship between the false alarm rate P_f and the detection threshold T is given by

$$\begin{aligned}
 P_f &= \int_T^\infty f_{KK}(x)dx = 1 - (1 - k)F_{K_1}(T) - kF_{K_2}(T) \\
 &= \frac{2 - 2k}{\Gamma(v)} \left(\frac{T}{2b}\right)^v K_v\left(\frac{T}{b}\right) + \frac{2k}{\Gamma(v_{sp})} \left(\frac{T}{2b_{sp}}\right)^{v_{sp}} K_{v_{sp}}\left(\frac{T}{b_{sp}}\right). \quad (18)
 \end{aligned}$$

The detection threshold T can be finally determined by (18). The equation defined in (18) includes modified Bessel function, which makes it complicated in its expression. Fortunately, the right side of the equation is a monotone function. Therefore, the threshold T can be solved easily.

In high-resolution SAR images, for 1) the corresponding extended target pixels in the binary image obtained from CFAR detector are generally not capable of forming a connected region and may be separated into several parts; 2) some smaller or larger regions in the binary image, which are obviously unsuitable for the size of a target region, will certainly cause false alarms; so it is necessary to cluster target pixels in the binary image. In [28], a detailed target pixels clustering method is presented. In this paper, this method is adopted to eliminate the obvious false alarms.

The CFAR detection flow chart is given in Fig. 6. In the flow chart, N_1 and N_2 denote the length and width of the input SAR image, x_{ij} is the amplitude of the pixels whose coordinate are (i, j) .

Figure 7 shows a typical high-resolution ground SAR image containing 12 vehicles in a complex urban clutter scene, which is collected in 2005 [28]. The airborne SAR platform operated at X-band and collected the data in stripmap mode HH polarization, with a resolution of $0.5\text{ m} \times 0.5\text{ m}$. The 12 vehicle targets are labeled in the image with white rectangles as show in Fig. 7. The parameter estimation results of the clutter models are given in Table 11. The amplitude histogram of the clutter is shown in Fig. 8 along with the four PDF of the clutter models. The goodness-of-fit tests, the chi-squared test and K-S test, are used again to demonstrate the performance of these clutter models. From Table 12, it can be seen that the KK is the best one of these four models.

The proposed global CFAR detection algorithm based on KK distribution proposed in this paper is employed to implement the vehicle targets detection task. The same detection algorithm based on G^0 distribution is also considered as a comparison. For the different false alarm $P_f = 10^{-5}$, $P_f = 10^{-4}$ and $P_f = 10^{-3}$, the detection results of the global detection algorithm based on KK distribution, and Figs. 9(g)–(m) show the detection results based on G^0 distribution

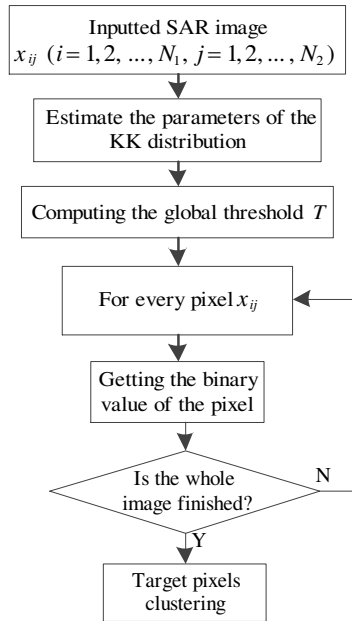


Figure 6. Detailed flow of the proposed target detection algorithm.

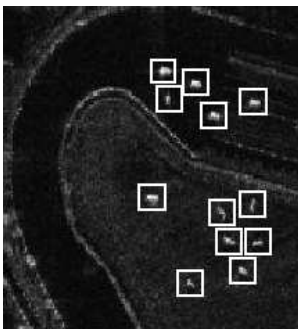


Figure 7. Ground SAR image containing vehicles.

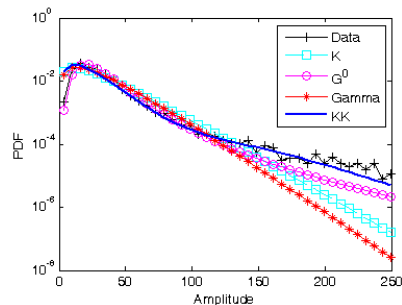


Figure 8. Amplitude histogram for image in Fig. 7.

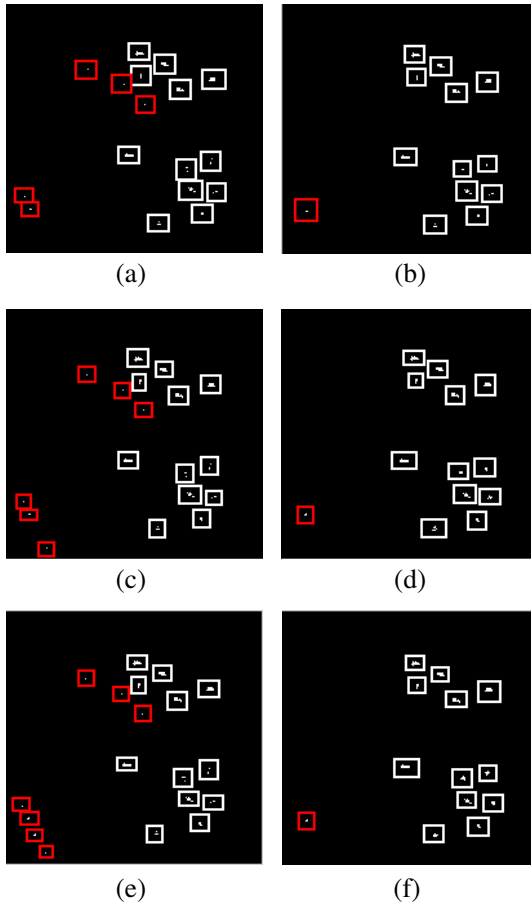
with the same false alarm rate. Binary images numbered (a), (c), (e), (g), (i), (k) give the detection results before target pixels clustering; and the detection results after pixels clustering are given in (b), (d), (f), (h), (j), (l). The detected results labeled with the white rectangles are the potential targets in Fig. 7. Meanwhile, the ones labeled with

Table 11. Parameter estimation results of the clutter models.

KK					K		G^0			Gamma	
\hat{k}	$\hat{\nu}_1$	$\hat{\nu}_2$	\hat{b}_1	\hat{b}_2	$\hat{\nu}$	\hat{b}	$\hat{\alpha}$	$\hat{\gamma}$	\hat{n}	\hat{a}	\hat{b}
0.0308	1.8439	6.6037	8.4551	18.8623	0.4042	26.2748	-2.2834	1432.5	1.9722	1.8722	14.2075

Table 12. Goodness-of-fit test for image in Fig. 7.

	K	G^0	Gamma	KK
K-S test	0.005287	0.005610	0.007378	0.002322
χ^2 test	5.0380	7.6510	12.2310	0.6935



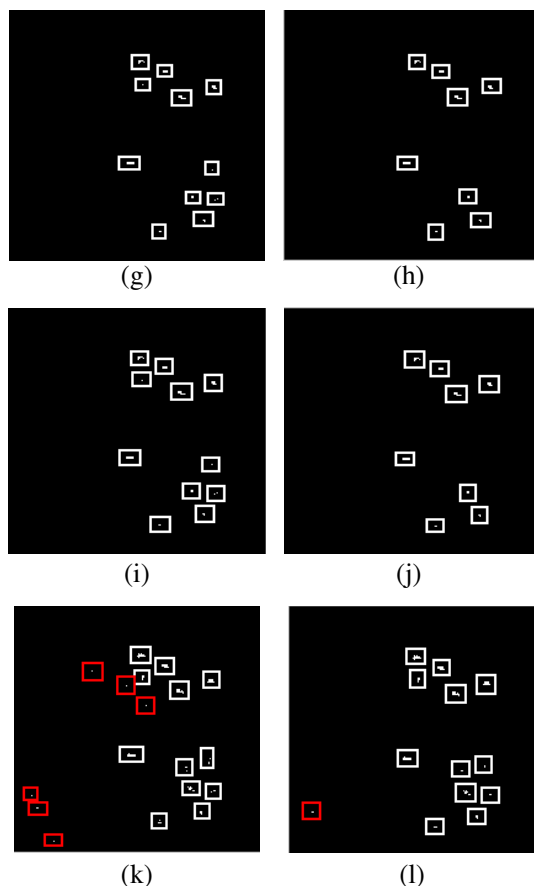


Figure 9. Results of target detection from an urban SAR image. (a), (c), (e) Detection results based on KK distribution with $P_f = 10^{-5}$, $P_f = 10^{-4}$, and $P_f = 10^{-3}$ (before clustering); (b), (d), (f) Detection results based on KK distribution with $P_f = 10^{-5}$, $P_f = 10^{-4}$, and $P_f = 10^{-3}$ (after clustering); (g), (i), (k) Detection results based on G^0 distribution with $P_f = 10^{-5}$, $P_f = 10^{-4}$, and $P_f = 10^{-3}$ (before clustering); (h), (j), (l) Detection results based on G^0 distribution with $P_f = 10^{-5}$, $P_f = 10^{-4}$, and $P_f = 10^{-3}$ (after clustering)

the red rectangles are false alarms.

From Figs. 9(a)–(f), the 12 vehicle targets in the SAR image are all well located using the CFAR detector based on KK distribution proposed in this paper with the theoretical false alarm probability

$P_f = 10^{-5}$, $P_f = 10^{-4}$ and $P_f = 10^{-3}$. The detection results in Fig. 9(a), Fig. 9(c), Fig. 9(e) also include 5, 6, 7 false alarms except for the true targets before pixels clustering, respectively. Most of the false alarms consist of very few pixels, which are obviously not unsuitable for the size of a target. Fig. 9(b), Fig. 9(d) and Fig. 9(f) show the detection results after pixels clustering. It is seen that most of the false alarms are eliminated successfully, which means that the clustering step in the detection algorithm is necessary. Correspondingly, Figs. 9(g)–(l) show the detection results based on G^0 distribution with the same false alarm probability. Both for false alarm rate $P_f = 10^{-5}$ and $P_f = 10^{-4}$, only 11 targets are detected before pixels clustering ((g) and (i)). Some of the detected targets consist of only one pixel because of the high detection threshold, which is caused by the improper choice of G^0 model. Three targets are lost in the pixels clustering, and only 8 targets are left in (h) and (j). From these detection results in Fig. 9, the proposed algorithm based on KK distribution has much better performance than the one based on G^0 distribution for the KK distribution is has a higher precision to fit the ground SAR images.

5. CONCLUSION

In this paper, a global CFAR target detection algorithm is presented for ground target detection in SAR image. The KK distribution is employed to model the ground SAR clutter in the algorithm. In order to obtain the precise parameter estimation of KK distribution, a novel algorithm based on PSO is firstly proposed and the simulation results based on simulated data sets generated under different conditions clearly show its superiority to the semi-experiential one in estimation performance. The KK distribution is then applied to model the SAR clutter data from MSTAR dataset, and the experimental results indicate that this mixture distribution has higher fitting precision than the commonly used models such as K distribution, Gamma distribution and G^0 distribution. The effectiveness of the proposed CFAR detection algorithm is finally validated by the test results for a typical real SAR image containing 12 vehicle targets.

ACKNOWLEDGMENT

This work was supported in part by the National Natural Science Foundation of China (Grant No. 61002022).

REFERENCES

1. Yan, W., J.-D. Xu, G. Wei, L. Fu, and H.-B. He, "A fast 3D imaging technique for near-field circular SAR processing," *Progress In Electromagnetics Research*, Vol. 129, 271–285, 2012.
2. An, D. X., Z.-M. Zhou, X.-T. Huang, and T. Jin, "A novel imaging approach for high resolution squinted spotlight SAR based on the deramping-based technique and azimuth NLCS principle," *Progress In Electromagnetics Research*, Vol. 123, 485–508, 2012.
3. Guo, D., H. Xu, and J. Li, "Extended wavenumber domain algorithm for highly squinted sliding spotlight SAR data processing," *Progress In Electromagnetics Research*, Vol. 114, 17–32, 2011.
4. Wei, S.-J., X.-L. Zhang, and J. Shi, "Linear array SAR imaging via compressed sensing," *Progress In Electromagnetics Research*, Vol. 117, 299–319, 2011.
5. Xu, W., P. Huang, and Y.-K. Deng, "Multi-channel SPCMB-tops SAR for high-resolution wide-swath imaging," *Progress In Electromagnetics Research*, Vol. 116, 533–551, 2011.
6. Novak, L. M., G. J. Owirka, and A. L. Weaver, "Automatic target recognition using enhanced resolution SAR data," *IEEE Transactions on Aerospace and Electronic Systems*, Vol. 35, No. 1, 157–175, 1999.
7. Wang, Y., Q. Song, T. Jin, X. Huang, and H. Zhang, "A novel minefield detection approach based on morphological diversity," *Progress In Electromagnetics Research*, Vol. 136, 239–253, 2013.
8. Lou, J., T. Jin, and Z. Zhou, "Feature extraction for landmine detection in UWB SAR via SWD and isomap," *Progress In Electromagnetics Research*, Vol. 138, 157–171, 2013.
9. Zhai, Y., J. Li, J. Gan, and Z. Ying, "A multi-scale local phase quantization plus biomimetic pattern recognition method for SAR automatic target recognition," *Progress In Electromagnetics Research*, Vol. 135, 105–122, 2013.
10. Teng, H. T., H.-T. Ewe, and S. L. Tan, "Multifractal dimension and its geometrical terrain properties for classification of multi-band multi-polarized SAR image," *Progress In Electromagnetics Research*, Vol. 104, 221–237, 2010.
11. Ren, S., W. Chang, T. Jin, and Z. Wang, "Automated SAR reference image preparation for navigation," *Progress In Electromagnetics Research*, Vol. 121, 535–555, 2011.
12. Di Bisceglie, M. and C. Galdi, "CFAR detection of extended objects in high-resolution SAR images," *IEEE Transactions on*

- Geoscience and Remote Sensing*, Vol. 43, No. 4, 833–843, 2005.
13. Ai, J., X. Qi, W. Yu, et al., “A new CFAR ship detection algorithm based on 2-D joint log-normal distribution in SAR images,” *IEEE Transactions on Geoscience and Remote Sensing Letters*, Vol. 7, No. 4, 806–810, 2010.
 14. Gao, G., “A parzen-window-kernel-based CFAR algorithm for ship detection in SAR images,” *IEEE Transactions on Geoscience and Remote Sensing Letters*, Vol. 8, No. 3, 557–561, 2011.
 15. Habib, M. A., M. Barkat, B. Aissa, and T. A. Denidni, “CA-CFAR detection performance of radar targets embedded in non-centered chi-2 gamma clutter,” *Progress In Electromagnetics Research*, Vol. 88, 135–148, 2008.
 16. Tian, B., D.-Y. Zhu, and Z.-D. Zhu, “A novel moving target detection approach for dual-channel SAR system,” *Progress In Electromagnetics Research*, Vol. 115, 191–206, 2011.
 17. Brekke, C. and S. N. Anfinsen, “Ship detection in ice-infested waters based on dual-polarization SAR imagery,” *IEEE Transactions on Geoscience and Remote Sensing Letters*, Vol. 8, No. 3, 391–395, 2011.
 18. Cui, Y., G. Zhou, J. Yang, and Y. Yamaguchi, “On the iterative censoring for target detection in SAR images,” *IEEE Transactions on Geoscience and Remote Sensing Letters*, Vol. 8, No. 4, 641–645, 2011.
 19. Budillon, A., A. Evangelista, and G. Schirinzi, “GLRT detection of moving targets via multibaseline along-track interferometric SAR systems,” *IEEE Transactions on Geoscience and Remote Sensing Letters*, Vol. 9, No. 2, 348–352, 2012.
 20. Zhang, G. and J.-F. Cao, “Application of extended fractal features in target sized objects detection of SAR image,” *Journal of Nanjing University of Aeronautics and Astronautics*, Vol. 36, No. 3, 378–382, 2004.
 21. Tello, M., C. López-Martínez, and J. J. Mallorqui, “A novel algorithm for ship detection in SAR imagery based on the wavelet transform,” *IEEE Transactions on Geoscience and Remote Sensing Letters*, Vol. 2, No. 2, 201–205, 2005.
 22. Zhang, J., G. Gao, D.-F. Zhou, and J.-J. Huang, “Comparison on two CFAR algorithms of vehicle target detection in SAR images,” *Signal Processing*, Vol. 24, No. 1, 78–82, 2008.
 23. Greco, M. S. and F. Gini, “Statistical analysis of high-resolution SAR ground clutter data,” *IEEE Transactions on Geoscience and Remote Sensing*, Vol. 45, No. 3, 566–575, 2007.

24. Zhao, Y. W., M. Zhang, X. P. Geng, and P. Zhou, "A comprehensive facet model for bistatic SAR imagery of dynamic ocean scene," *Progress In Electromagnetics Research*, Vol. 123, 427–445, 2012.
25. Albert, M. D., Y. J. Lee, H. T. Ewe, and H. T. Chuah, "Multilayer model formulation and analysis of radar backscattering from sea ice," *Progress In Electromagnetics Research*, Vol. 128, 267–290, 2012.
26. Bausssard, A., M. Rochdi, and A. Khenchaf, "PO/Mec-based scattering model for complex objects on a sea surface," *Progress In Electromagnetics Research*, Vol. 111, 229–251, 2011.
27. Frery, A. C., H.-J. Müller, et al., "A model for extremely heterogeneous clutter," *IEEE Transactions on Geoscience and Remote Sensing*, Vol. 35, No. 3, 648–659, 1997.
28. Gao, G., L. Liu, L. Zhao, G. Shi, and G. Kuang, "An adaptive and fast CFAR algorithm based on automatic censoring for target detection in high-resolution SAR images," *IEEE Transactions on Geoscience and Remote Sensing*, Vol. 47, No. 6, 1685–1697, 2009.
29. Dong, Y., "Distribution of X-band high resolution and high grazing angle sea clutter," Defense Science and Technology Organisation, 2006.
30. Ward, K. D., "Compound representation of high resolution sea clutter," *Electronics Letters*, Vol. 17, No. 16, 561–563, 1981.
31. Watts, S., "Radar detection prediction in K-distributed sea clutter and thermal noise," *IEEE Transactions on Aerospace and Electronic Systems*, Vol. 23, No. 1, 40–45, 1987.
32. Skolnik, M. I., *Introduction to Radar Systems*, 3rd Edition, McGraw-Hill, New York, 2008.
33. Ward, K. D. and R. J. A. Tough, "Radar detection performance in sea clutter with discrete spikes," *International Radar Conference*, 253–257, 2002.
34. Watts, S., K. D. Ward, and R. J. A. Tough, "The physics and modeling of discrete spikes in radar sea clutter," *Proc. of International Radar Conference*, 2005.
35. Anfinson, S. N. and T. Eltoft, "Application of the matrix-variate Mellin transform to analysis of polarimetric radar images," *IEEE Transactions on Geoscience and Remote Sensing*, Vol. 49, No. 6, 2281–2295, 2011.
36. Kennedy, J. and R. Eberhart, "Particle swarm optimization," *Proc. of the IEEE International Conference on Neural Networks*, 1942–1948, 1995.

37. Cui, X., T. Potok, and P. Palathingal, "Document clustering using particle swarm optimization," *Proc. of the 2005 IEEE on Swarm Intelligence Symposium*, 185–191, 2005.
38. Ren, Z. and J. Wang, "New adaptive particle swarm optimization algorithm with dynamically changing inertia weight," *Computer Science*, Vol. 2, No. 36, 227–229, 2009.
39. Shi, Y. and R. C. Eberhar, "Empirical study of particle swarm optimization," *Proc. of the 1999 IEEE on Evolutionary Computation*, 1945–1948, 1999.
40. Roberts, W. J. J. and S. Furui, "Maximum likelihood estimation of K-distribution parameters via the expectation-maximization algorithm," *IEEE Transactions on Signal Processing*, Vol. 48, No. 12, 3303–3306, 2000.
41. Anastassopoulos, V., G. A. Lampropoulos, A. Drosopoulos, and M. Rey, "High resolution radar clutter statistics," *IEEE Transactions on Aerospace and Electronic Systems*, Vol. 35, No. 1, 43–60, 1999.
42. Li, H.-C., W. Hong, Y.-R. Wu, and P.-Z. Fan, "An efficient and flexible statistical model based on generalized Gamma distribution for amplitude SAR images," *IEEE Transactions on Geoscience and Remote Sensing*, Vol. 48, No. 6, 2711–2722, 2010.
43. Weinberg, G. V., "An investigation of the Pareto distribution as a model for high grazing angle clutter," Electronic Warfare and Radar Division Defense Science and Technology Organization, 2011.